



Plume Interaction and Base Flow Analysis of a Twin Engine Flight Vehicle

Mamidi Sri Rama Chandra Murty¹ · Debasis Chakraborty¹

Received: 24 November 2014 / Accepted: 18 May 2016 / Published online: 17 June 2016
© The Institution of Engineers (India) 2016

Abstract 3D RANS simulations are performed to study the multi jet interactions of a twin engine gimbal configuration of an aerospace vehicle at different time instants. Simulations captured all the essential features of the flow field and interaction between the neighboring jets did not occur because of low altitudes and moderate under-expansion of the jets considered in the simulations. For higher gimbal angle, two jets were the closest but still did not interact. Detail exploration of the downstream flow field revealed that the distinct features of the jets are retained at the farthest downstream locations; although the pressure field reached the uniformity. Average base pressure ratios for the three different time instances are 0.91, 0.547 and 0.522 and maximum base temperature is of the order 800 K.

Keywords Convective base heating · Multijet interaction · RANS

Introduction

The energy transfer from the rocket exhaust to the vehicle base in missiles and satellite launch vehicles during the ascent phase in the atmosphere causes one of the most complex aerothermodynamics problems—the base heating. For range extension and payload increase, flight vehicles use multi-nozzle clusters and or strap-on motors in the lower stages. The plumes of these rocket motors

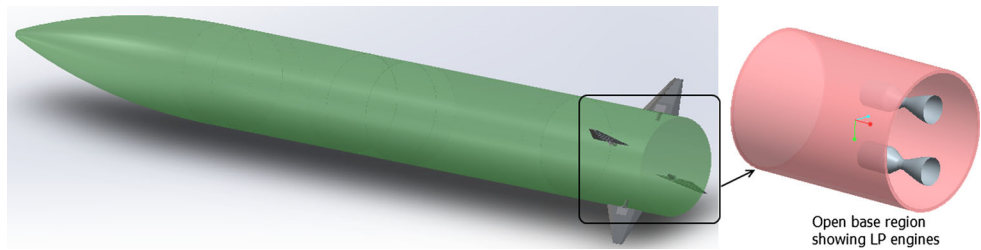
become more and more under-expanded and bulge in size with the increase in altitude. These expanding plumes interact with each other and also with external free stream and cause the hot rocket exhaust to recirculate towards the base of the vehicle resulting in base heating and higher base pressure. The recirculation flow also changes the base drag and has significant effect on the mission performance. Different launch vehicles (Titan, Space Shuttle, Ariane etc.) have experienced complex base flow and consequent base heating in their early flight campaigns. Experimental investigations [1–3] have revealed many features of this complex problem and provided sufficient design information [4] so that the detrimental effect of base heating is largely avoided in operational vehicles.

The interaction of rocket exhaust and free stream flow continues to be an active research problem for fundamental flow physics as well as for engineering applications. The role of unsteady vortex shedding and large coherent structure in the supersonic base flow and their impact on the mean flow is far from understood. The base flow parameters are such a strong function of engine configuration, vehicle trajectory, base geometry and engine operating conditions so that the base heating rate of two different flight vehicles can vary on order of magnitude. Understanding of the mechanism involved in the energy transfer and quantitative estimation of recirculation flow properties are very important for structural and thermal design of base shroud of any flight vehicle. Base flow aerodynamics is treated by two kinds of calculation methods (1) semi-empirical multicomponent approach of Chapman and Korst [5, 6] and (2) the solution of the time averaged Navier–Stokes equation with turbulence closure [7–14]. Although the semi-empirical approaches demonstrated their validity in many 2D/axisymmetric configurations, its application is not always reliable for

✉ Debasis Chakraborty
debasis.drld@yahoo.co.in

¹ Defence Research and Development Laboratory, Hyderabad 500058, Telangana, India

Fig. 1 The schematic view of the aerospace vehicle with highlighted based region



complex 3D geometries. Moreover, simpler correlations can predict only one average value of the base flow parameters in the whole region which is often found to be inadequate for design calculations.

With the advent of powerful computers and robust numerical algorithms, the solution of 3D RANS equations with appropriate turbulence models are routinely used in the calculation of multijet base flow problems in aerospace industry. Sahu et al. [8] simulated the experimental condition of Herrin and Dutton [15] and predicted the radial variation of base pressure. This study reveals the predicted base pressure with $k-\varepsilon$ turbulence model is closer to the experimental value in comparison with other algebraic turbulence models. Chakraborty et al. [11] simulated axisymmetric base flow experiment of Reid and Hastings [16] for different pressure ratios of free stream and propulsion jets. A grid adaptive Cartesian mesh based Navier–Stokes solver with $k-\varepsilon$ turbulence model was used and a qualitative match of computational base pressures with experimental values was obtained. Dharavath et al. [13] simulated the experimental condition of supersonic base flow conducted at University of Delft, Netherlands by Bannink et al. [17] by solving 3D RANS equations in unstructured mesh using commercial software and brought out the effect of computational grid and turbulence model in predicting the radial variation of base pressure. In the present work numerical simulations are presented to study the base flow arising due to interaction between the plumes of two liquid fuelled gimball engines with each other and also with the coflowing free stream at different instances of time.

Vehicle Geometry and Inflow Parameters

The schematic view of the aerospace vehicle is presented in Fig. 1. It uses two liquid fuelled gimball engines which are deflected to control pitch, yaw and roll motion of the missile. The base region with two cluster engine is also highlighted in the figure. Simulations are carried out for three different instants. The flow conditions (static pressure, static temperature and Mach number) pertaining to free-stream and twin engine chamber conditions (total pressure P_0 and total temperature T_0) for these

Table 1 Inflow parameters and rocket exhaust properties

Parameters	Time		
	T1	T2	T3
Free stream parameters			
Free stream Mach number (M_∞)	0.38	0.90	1.10
Ambient pressure (p_∞), KPa	89	59	57
Ambient temperature (T_∞), K	295	270	258
Rocket exhaust properties			
Engine 1 chamber pressure (p_0), MPa	5.77	5.81	5.81
Engine 2 chamber pressure (p_0), MPa	5.66	5.81	5.85
Chamber temperature T_0 , K	3065	3065	3065
Ratio of specific heat	1.213	1.213	1.213
Molecular weight, kg-mole/ m^3	24.14	24.14	24.14
Pressure ratio (p_j/p_∞)	1.12	2.31	2.15
Gimball angles for engine at various instants			
Engine 1 (x–y plane)	0.87	2.74	0.10
Engine 1 (x–z plane)	0.94	–0.28	0.08
Engine 2 (x–y plane)	0.96	2.89	0.53
Engine 2 (x–z plane)	0.54	–0.31	0.03

instants are presented in Table 1. The free stream Mach number of vehicle trajectory ranges from subsonic (0.39) to low supersonic (1.10) values. There are very marginal differences between the chamber conditions of two engines. The engines are gimballed in pitch, yaw direction by small amount ranging from 0 to 2 degrees for vehicle control.

Computational Methodology

Simulations are carried out using commercial CFD software Ansys Fluent 14.5 [18]. It solves three-dimensional Navier–Stokes equation in an unstructured, hybrid grid system using a collocated variable arrangement. To simulate high Mach number compressible flow (as in the present case), density band solver is used along with Roe Flux difference splitting scheme [19] for spatial discretization and 1st order implicit Euler scheme for temporal

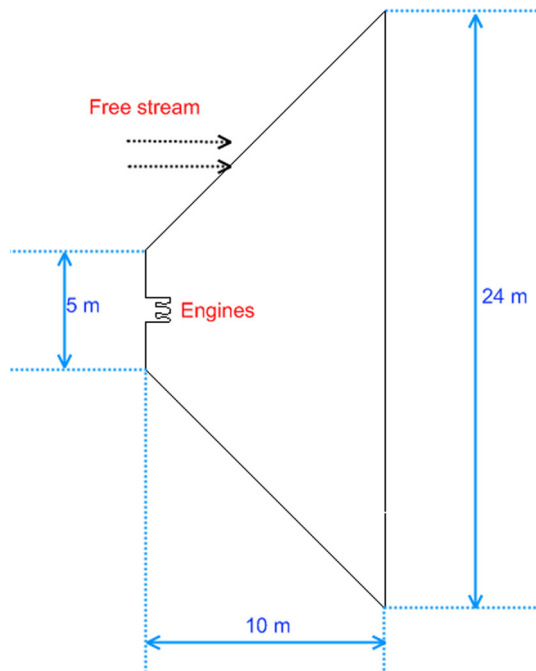


Fig. 2 The computational domain

discretization. Turbulence is modeled using $k-\epsilon$ turbulence model along with wall function. The chamber conditions are imposed at the nozzle inlet plane whereas free-stream flow conditions are prescribed at free stream inflow. Pressure boundary condition is prescribed at far-field and outflow boundary condition. Adiabatic condition for temperature and no slip condition for velocity are imposed on all the walls. The computational methodology has been validated extensively for different non-reacting high speed propulsion problems including jet vane characterization of long range surface to air missile [20], design of plume

Table 2 Comparison of parameters between two different grids

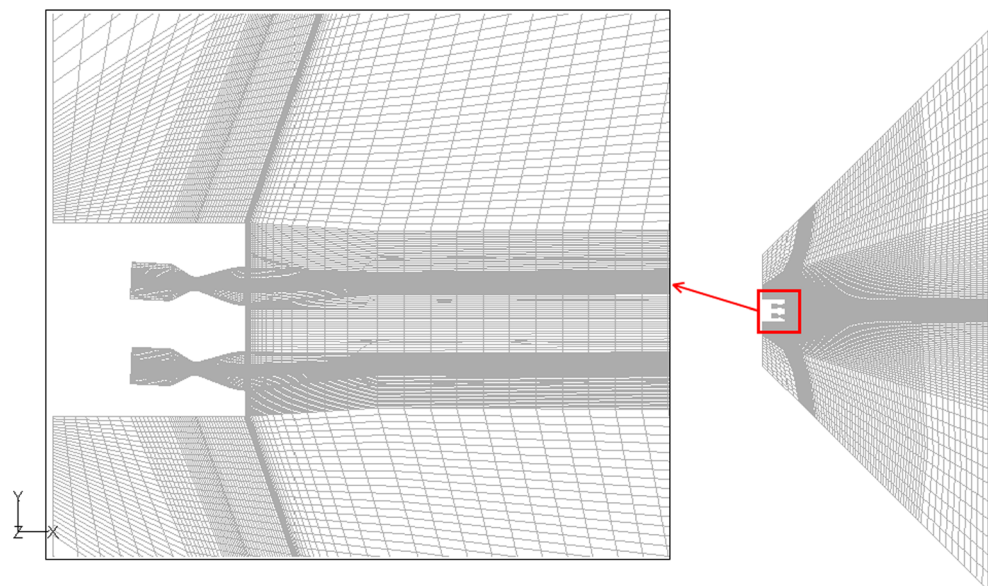
Parameters	Mesh-1 (1.75 m cells)	Mesh-2 (3.49 m cells)	% difference
Average base pressure, ksc	0.23	0.24	2.05
Average base temperature, K	665.06	614.83	7.55
Skin friction coefficient	79.09	72.43	8.42

ducting system of ship launched missile [21], hypersonic air intake flow field [22] etc.

Results and Discussions

The computational domain of flow field is shown in Fig. 2. The inflow boundary of the computational domain is placed at a distance of one base diameter (1 m) upstream of the base. Nozzle inlet plane is considered as the inflow plane for engines. The far-field boundary is 2.5 and 12 m in upward direction at inflow plane and outflow planes respectively. The outflow boundary is taken 10 m downstream of the base in the axial direction. The hexahedral grid is generated in the computational domain using ICEM CFD [23] grid generator. Grids are clustered near the wall and also in the jet shear layer. Typical grid is shown in Fig. 3. Two grids of sizes 1.75 million cells and 3.5 million cells have been made for grid variation study. Average base pressure, temperature and the skin friction coefficient on the wall for these two grids are presented in Table 2. It can be seen that change of grid has given only marginal change in base pressure values. Further simulations are performed with fine grid distribution.

Fig. 3 Computational mesh with exploded view near the base region



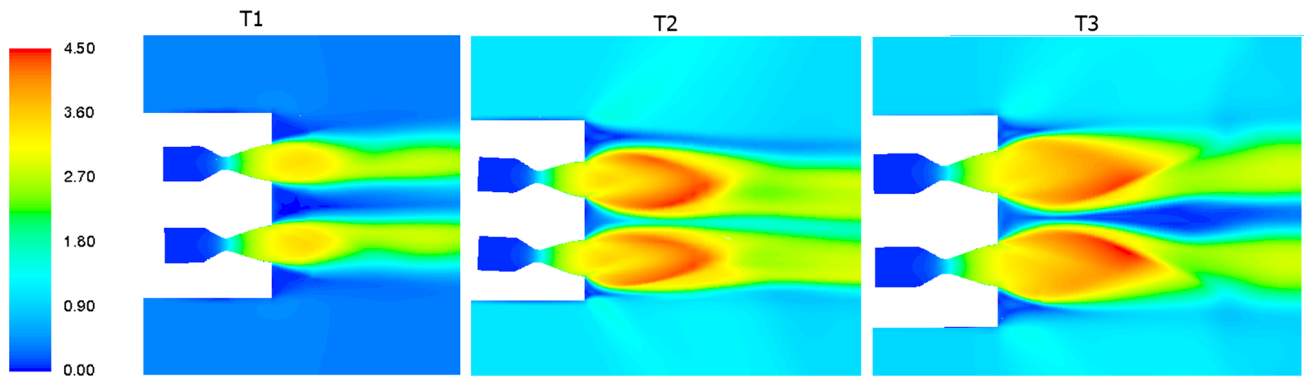
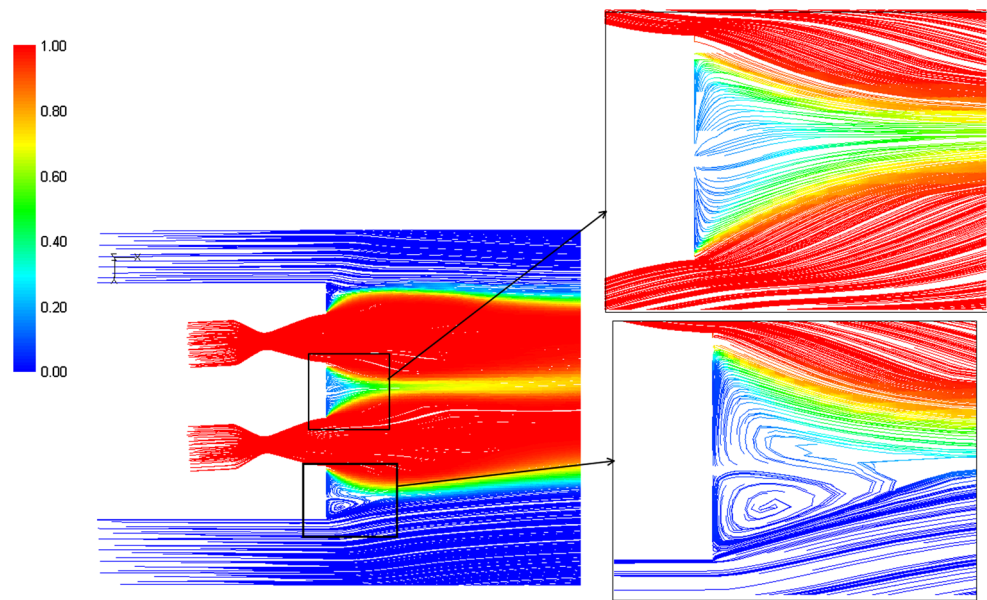


Fig. 4 Mach number contour in x - y plane ($z = 0$) for cases T1, T2 and T3

Fig. 5 Streamlines plot at 38 s (coloured by hot gas mass fraction)



The Mach number contour in the x - y plane ($z = 0$) for three different instants are shown in Fig. 4. With the increase in the altitude, jets are bulging more. Shear layers formed at the free-stream-jet interface and the expansion fan at the shoulder of the vehicle are clearly visible in these figures. At T2 time instant, since both the engines are deflected towards each other at higher angles, jet boundaries came closest. Yet, no recompression shock (which is indicative of jet interaction) appeared. To illustrate this point further, streamline pattern coloured by hot gas mass fraction for T2 time instant is shown in Fig. 5. The zoomed view in both upper and central region did not show any hot gas recirculation at the base. The difference in the flow pattern between the upper and lower part of the base is due to the different gimbaling of the engine. The computed base pressure at the middle part is shown to be higher than that of bottom part as shown in the radial variation plot in Fig. 6. The pressure profiles at different axial locations ($X/D = 1, 1.5, 2$ and 2.5) for time instants T2 and T3 in

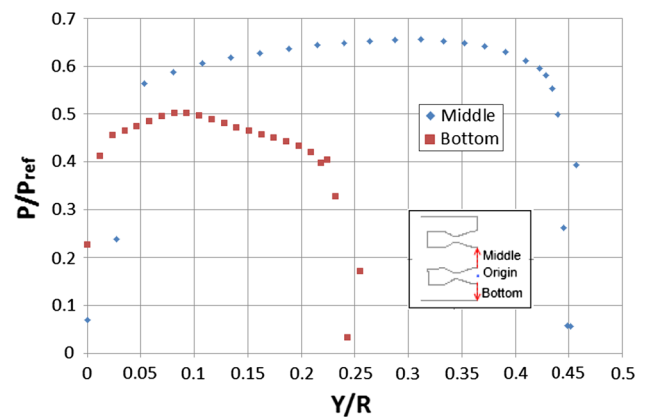


Fig. 6 Base pressure variation radial direction

downstream region are presented in Fig. 7 where, D is missile base diameter. The non-uniformity of pressure in the nearwake region has almost disappeared at $X/D = 2.5$ axial location. The nondimensionalised velocity (U/U_j) and

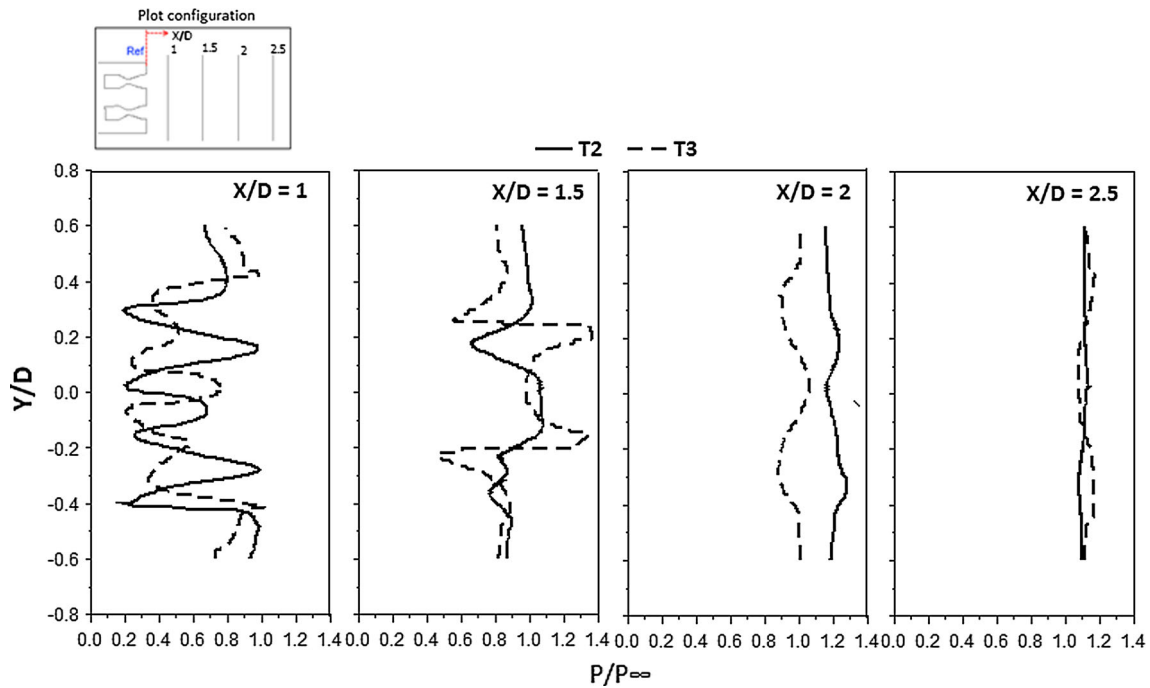


Fig. 7 Plume pressure profiles in radial direction at different axial stations

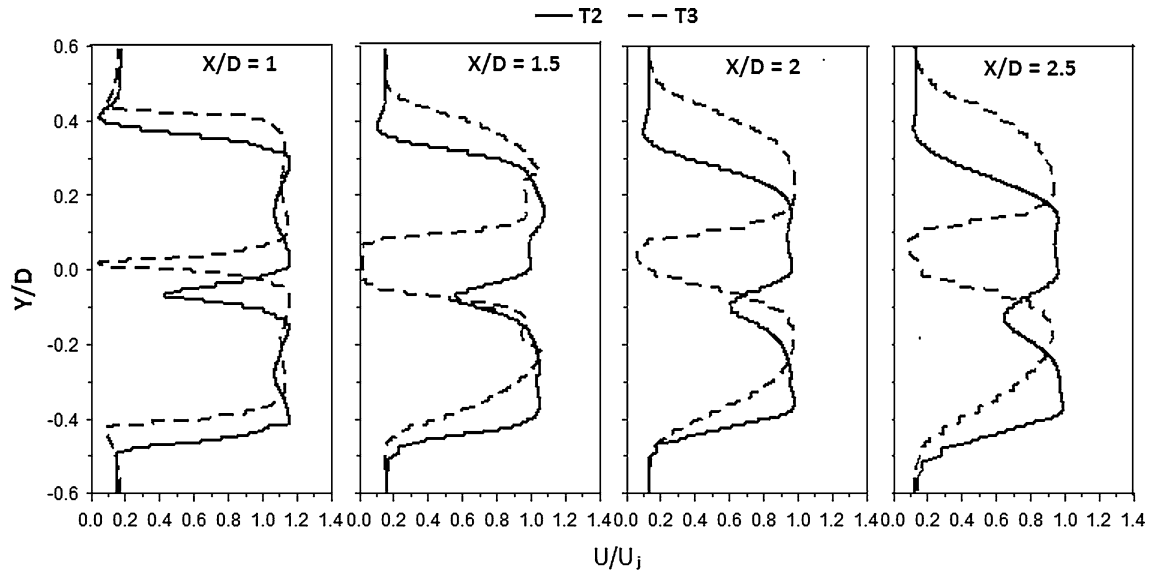


Fig. 8 Plume velocity profiles in radial direction at different axial stations

temperature profiles (T/T_j) in different axial locations are presented in Figs. 8 and 9 respectively (U_j and T_j are the velocity and temperature at the jet exit). It can be observed that although the pressure profiles are becoming uniform at $X/D = 2.5$, the two jets retained their distinct features even in the location of $X/D = 2.5$. It is also observed that at T2 time instants, the jet profiles are more uniform compared to T3 instants. It is due to the maximum gimballing of the two jets towards each other at T2 instants. The base gas

temperature is found to be highest (~ 800 K) for T2 case. The average base pressure (p_b/p_∞) ratios for all the three instants are 0.91, 0.547 and 0.522 respectively. The azimuthal variation of pressure (p/p_∞) and Mach number at $x/D = 1$ for T2 instant is presented in Fig. 10. The azimuthal angle (θ) starts from Y^+ axis in the pitch plane and increases in counterclockwise direction. Significant variation of flow parameters are observed at $\theta = 180^\circ$ (Y^- axis in the pitch plane) due to engine gimballing.

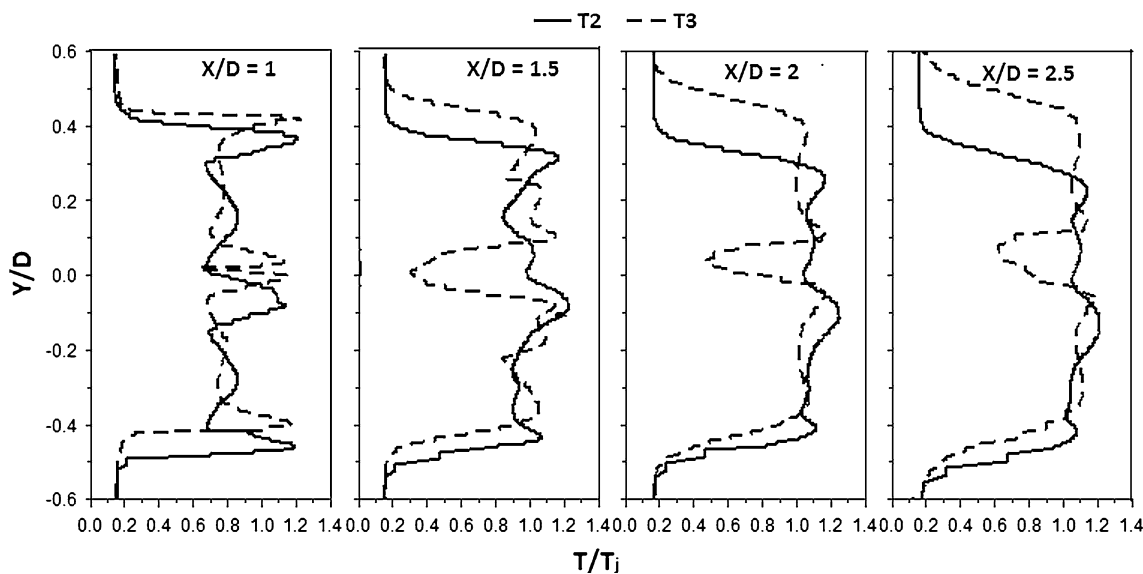


Fig. 9 Plume temperature profiles in radial direction at different axial stations

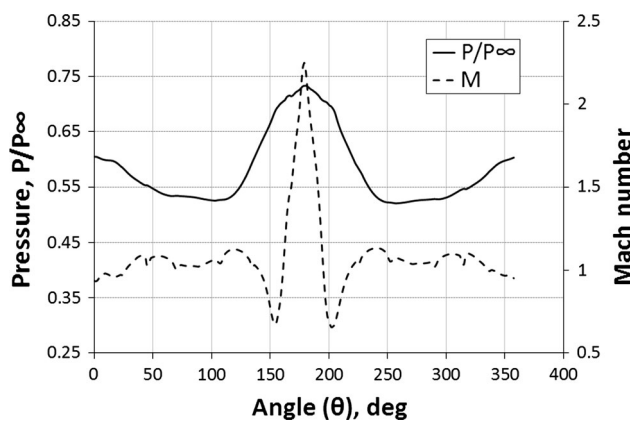


Fig. 10 Azimuthal variation of pressure and Mach number at $x/D = 1$

Conclusions

Multijet interaction of a twin engine gimbal configuration is simulated numerically at different flight instants. Three dimensional Navier–Stokes equations are solved along with $k-\epsilon$ turbulence model using commercial CFD software. Grid independence of the solution has been demonstrated by carrying simulation with two different grids and comparing the average base pressure and skin friction coefficients. The flow fields are analyzed in detail to find out the interaction between the neighbouring jets and consequent recirculation of hot gases. Since the altitudes are low and the jets are moderately under-expanded, the bulging of the jets are limited and the jet interactions are not found for any of the three instants considered for simulations. For higher gimbal angle, two jets were the closest but still did not interact. Detail exploration of the

downstream flow field revealed that the distinct features of the jets are observed from velocity and temperature profiles even at farthest downstream locations of $x/D = 2.5$; although the pressure field reached the uniformity. Average base pressure ratios for the three different time instances are 0.91, 0.547 and 0.522 and maximum base temperature is of the order 800 K.

References

1. B.H. Goethert, R.J. Matz, Experimental investigation of base flow characteristics of four-nozzle cluster-rocket models. The Fluid Dynamic aspects of Space Flight, AGARADograph No. 87, vol. 2, (1966), pp. 223–244
2. R.J. Sargent, Base heating scaling criteria for a four engine Rocket Cluster operating at high altitudes. AIAA Paper, pp. 65–826
3. R.A. Wasko, T.L. Cover, Experimental investigation of base flow field at high altitudes for configurations of four and five clustered nozzles. NASA-TMX–1371, (1967)
4. G.A. Etemad, K.D. Korken, Base flow characteristics and thermal environment of launch vehicle with strap on solid rocket motors. J. Astronaut. Sci. **15**(1), 5–13 (1968)
5. D.R. Chapman, An analysis of base pressure at supersonic velocities and comparison with experiments. NACA Report 1051, (1951)
6. H.H. Korst, A theory of base pressure in transonic and supersonic flow. J. Appl. Mech. **23**, 593–600 (1956)
7. G.S. Deiwert, Supersonic axisymmetric base flow over boattails containing a central propulsive jets. AIAA J. **22**, 1358–1365 (1984)
8. J. Sahu, C. Nietubicz, J. Steger, Navier-Stokes computations of projectile base flow with and without mass injection. AIAA J. **23**(9), 1348–1355 (1985)
9. J. Sahu, Numerical computation of supersonic base flow with special emphasis on turbulence modelling. AIAA J **32**(7), 1547–1549 (1994)

10. E.M. Houtman, V.D. Weide, E. Deconinck, P.G. Bakker, Computational analysis of base flow/jet plume interaction, in Proceeding of 3rd European Symposium on Aerothermodynamics for Space Vehicles, ESA SP-426, pp. 605–612, (1998)
11. D. Chakraborty, P. Kumar, R. Balu, V. Adimurthy, Numerical simulation of axisymmetric base flow in the presence of propulsive Jet. *J. Aeronau. Soc. India* **53**(1), 35–38 (2001)
12. P.G. Bakker, W.J. Bannink, P. Servel, P. Reijasse, *CFD validation for base flows with and without plume interaction*. AIAA 2002–0438, 40th Aerospace sciences meeting and exhibit, Reno, 14–17 January 2002
13. M. Dharavath, P.K. Sinha, D. Chakraborty, Simulation of supersonic base flow—effect of grid and turbulence model, in Proceedings of IMechE, vol 224, Part G: J Aerospace engineering, (2009), pp. 311–319
14. S. Saha, S. Rathod, M.S.R. Chandra Murty, P.K. Sinha, D. Chakraborty, Numerical simulation of base flow of a long range flight vehicle. *Acta Astronaut.* **74**(3), 112–119 (2012)
15. J.L. Herrin, J.C. Dutton, Supersonic base flow experiments in the near wake of a cylindrical afterbody. *AIAA J.* **32**(1), 77–83 (1994)
16. J. Reid, R.C. Hastings, The effect of a central jet on the base pressure of a cylindrical after-body in a supersonic stream. Aeronautical Research Council (Great Britain) Reports and Memoranda No. 3224, (1959)
17. W.J. Bannink, P.G. Baker, E.M. Houtman, FESTIP aerothermodynamics: experimental investigation of base flow and exhaust plume interaction. Memorandum M-775, Aerospace Engineering, Delft University of Technology, (1997)
18. *Ansys Fluent 14.5 theory and users guide* (Ansys Inc, USA, 2012)
19. P.L. Roe, Characteristic based schemes for the Euler equations. *Annu. Rev. Fluid Mech.* **18**, 337–365 (1986)
20. M.S.R. Chandra Murty, M. Sambasiva Rao, D. Chakraborty, Numerical simulation of nozzle flow field with jet vane thrust vector control. *J. Aerosp. Eng.* **224**(5), 541–548 (2010)
21. S. Saha, D. Chakraborty, Plume ducting system design of vertical launcher using CFD tools. *J. Spacecr. Rockets* **50**(3), 715–718 (2013)
22. S. Saha, D. Chakraborty, Hypersonic Intake starting characteristics—a CFD validation study. *Def. Sci. J.* **62**(3), 147–152 (2012)
23. *User Manual, ICEM-CFD 14.5* (Ansys Inc, USA, 2012)